Density Functional Calculations

Models of High-Valent Intermediates of Non-Heme Diiron Alkane Monooxygenases: Electronic Structure of a Bis(μ-oxo)diron(IV) Complex with Locally Low-Spin Metal Centers**

Abhik Ghosh, Espen Tangen, Emmanuel Gonzalez, and Lawrence Que, Jr.**

Long known as a common structural unit in inorganic chemistry, the bis(μ-chalcogeno)dimetal "diamond" core is increasingly recognized as important in a biological context.[1,2] Thus, a variety of clusters based on $\{Fe_2(\mu\text{-}S)_2\}$ rhombs occur in iron–sulfur proteins and are involved in redox reactions, while intermediates with $\{M_2(\mu\text{-}O)_2\}$ cores have been implicated more recently for non-heme metalloenzymes involved in oxygen metabolism.[1,2] For example, $\{Mn_2(\mu\text{-}O)_2\}$ units have been identified as components of the tetramanganese cluster involved in photosynthetic oxygen evolution,[3] while $\{Cu^{III}{}_2(\mu\text{-}O)_2\}$ intermediates have been recently synthesized and postulated as intermediates in the catalytic cycles of copper oxygenases such as particulate methane monooxygenase.[2,4] Strong evidence for a high-valent $\{Fe^{IV}{}_2(\mu\text{-}O)_2\}$ core has also been found for the key methane-hydroxylating intermediate **Q** of soluble methane monooxygenase (sMMO).[5,6] A related Fe^{III}–Fe^{IV} species called intermediate **X** produces the catalytically essential tyrosyl radical in the R2 protein of ribonucleotide reductase to initiate the process of ribonucleotide reduction in DNA biosynthesis.[7] By analogy, high-valent $\{Fe^{IV}{}_2(\mu\text{-}O)_2\}$ intermediates are also proposed for other non-heme diiron alkane-oxidizing enzymes such as fatty acid desaturases[8] and the membrane-bound ω-hydoxylase AlkB.[9]

In recent years, a number of synthetic complexes with $\{Fe_2(\mu\text{-}O)_2\}^{n+}$ ($n=3$ or 4) cores and tetradentate N_4 capping ligands have been isolated and characterized; these serve as models of the enzymatic intermediates **Q** and **X**. With the tpa ligand (tpa = tris(2-pyridylmethyl)amine) and its 5-alkyl derivatives, the complexes with an $\{Fe_2(\mu\text{-}O)_2\}^{3+}$ core exhibit an $S=3/2$ ground state (S is the total spin angular momentum).[10,11] Mössbauer spectroscopy indicated that the two iron centers in these species are electronically identical, thus suggesting a valence-delocalized diiron(III,IV) description for the dinuclear center.[10] Density-functional theory (DFT) calculations further indicated that the individual iron centers in these complexes could be described as locally low-spin.[12] More recently, the first synthetic $\{Fe^{IV}{}_2(\mu\text{-}O)_2\}$ intermediate has been reported,[13] which provides the closest synthetic model so far of **Q**. However, while **Q** has a carboxylate-rich ligand environment and antiferromagnetically coupled, locally high-spin Fe^{IV} centers,[14] the synthetic model is paramagnetic ($S=1$), features relatively strong-field *N*,*N*′-bis(2-pyridylmethyl)-*N*,*N*′-dimethyl-*trans*-1,2-diaminocyclohexane (bpmcn) terminal ligands and presumably low-spin Fe^{IV} centers.[13] Such an $\{Fe^{IV}{}_2(\mu\text{-}O)_2\}$ intermediate with locally low-spin iron centers may actually be involved in the catalytic cycle of the alkane ω-hydroxylase AlkB, which is thought to have a histidine-rich ligand environment.[15] Because of its importance, the catalytic cycle of sMMO has been the subject of several quantum-chemical studies.[16,17,18] To complement these efforts, we have undertaken a DFT study of an $\{Fe^{IV}{}_2(\mu\text{-}O)_2\}$ model complex with locally low-spin iron centers.

By using nonlocal DFT[19,20] as implemented in the ADF[21] program system, the VWN local exchange-correlation functional, PW91 gradient corrections for both exchange and correlation, triple-ζ plus polarization Slater-type basis sets, and a fine mesh for numerical integrations of matrix elements, we carried out full geometry optimizations of $[(bipy)_2Fe(\mu\text{-}O)_2Fe(bipy)_2]^{4+}$ (bipy = 2,2′-bipyridyl) for the lowest-energy $S=1$ and 2 electronic states and also of $[(bipy)_2Fe(\mu\text{-}O)_2Fe(bipy)_2]^{3+}$ for its $S=3/2$ ground state. Use of the bipy ligand instead of the bpmcn ligand used in the synthetic modeling studies permitted us to exploit D_2 symmetry in each of these calculations. We also carried out similar calculations with D_{4d} symmetry constraints on the high-valent nitrido-bridged heme dimer complexes $[(por)Fe]_2N$ ($S=1/2$)[22] and $[\{(por)Fe\}_2N]^+$ ($S=0$)[23] (por = porphyrinato) which feature the same formal metal oxidation states as $[(bipy)_2Fe(\mu\text{-}O)_2Fe(bipy)_2]^{3+}$ and $[(bipy)_2Fe(\mu\text{-}O)_2Fe(bipy)_2]^{4+}$, respectively. A spin-restricted formalism was used for $[\{(por)Fe\}_2N]^+$, a closed-shell species,[23] while spin-unrestricted calculations were used for all the other complexes.

Figure 1 presents the Kohn–Sham molecular orbital (MO) energy levels in the Fe 3d "band" of each of the three $\{Fe_2(\mu\text{-}O)_2\}$ species studied. Figure 2 provides pictorial representations of some of these MOs. Figure 1 reveals a substantial energy separation between the t_{2g} and e_g bands, with only the t_{2g} band populated, thus indicating the low-spin nature of the iron centers in the species studied. Note also that the t_{2g} band is fairly densely spaced, which provides a simple explanation for the $S=3/2$ ground state of $[(bipy)_2Fe(\mu\text{-}O)_2Fe(bipy)_2]^{3+}$ in terms of filling six MOs with nine 3d electrons according to Hund's rules.[12] Not surprisingly, the $S=1$ and $S=2$ states of

[*] Prof. Dr. A. Ghosh, E. Tangen, E. Gonzalez
Department of Chemistry
University of Tromsø
N-9037 Tromsø (Norway)
Fax: (+47) 77644765
E-mail: abhik@chem.uit.no
Prof. Dr. L. Que, Jr.
Department of Chemistry and the Center for Metals in Biocatalysis
University of Minnesota, Minnespolis
MN 55455 (USA)
Fax: (+1)612 6247029
E-mail: que@chem.umn.edu

[**] This work was supported by the Norwegian Research Council (AG), the VISTA program of Statoil (Norway) and of the Norwegian Academy of the Sciences and Letters (AG), a Senior Fellowship of the San Diego Supercomputer Center (AG), a Socrates/Erasmus scholarship (EM), and grant no. GM-38767 of the US National Institutes of Health (LQ).

Supporting information for this article is available on the WWW under http://www.angewandte.org or from the author. Optimized Cartesian coordinates of the molecules studied in this work are available.

  DOI: 10.1002/anie.200351768

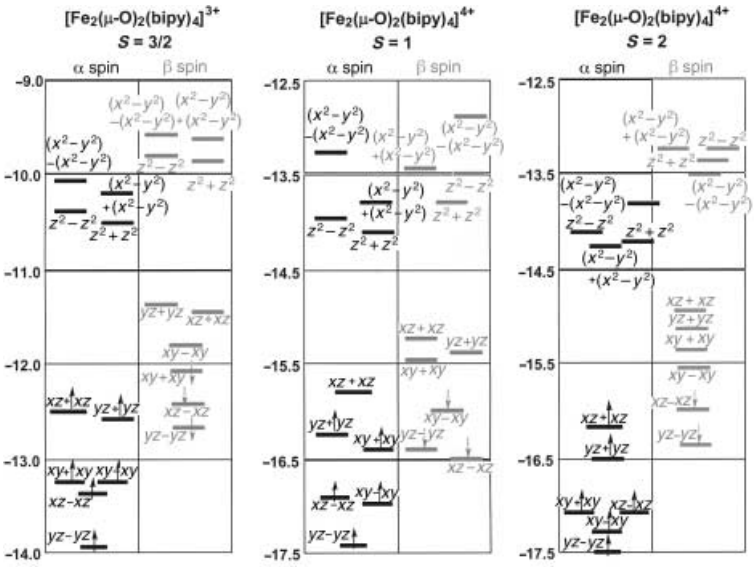

Figure 1. MO energy level diagrams for $\{Fe_2(\mu\text{-}O)_2\}$ model complexes studied. The energy scale is in eV. The orbital energies of these MOs are listed in the Supporting Information.

$[(bipy)_2Fe(\mu\text{-}O)_2Fe(bipy)_2]^{4+}$ are found to be comparable in energy, with the triplet state 0.18 eV above the quintet state. Although a triplet ground state has been found for the model complex studied experimentally,[13] the energy difference of 0.18 eV is at or below the threshold of the accuracy with which DFT can currently describe energy differences between spin states of transition-metal compounds.[24] By comparison, the $S=0$ state, which we also examined lies above the ground state by a substantial margin of 0.84 eV,[25] exhibits a distinctly non-aufbau orbital energy spectrum and is clearly excluded as a possible candidate as the ground state. Apparently, the dense spacing of the t_{2g} band discourages maximum spin pairing of the Fe 3d electrons, which is one of the key insights provided by these calculations.

Figure 3 presents MO energy-level diagrams for $[\{(por)Fe\}_2N]$ and $[\{(por)Fe\}_2N]^+$ and Figure 4 depicts some of these MOs pictorially. The linear Fe-N-Fe arrangement[22,23] in these compounds reflects strong Fe-N-Fe π-bonding resulting in much larger energy splittings within the t_{2g} bands in these compounds (Figure 4) compared with the $\{Fe_2(\mu\text{-}O)_2\}$ complexes described above. These band gaps result in maximum pairing of the Fe electron spins in the nitrido-bridged heme dimers. A similar scenario also holds for carbido-bridged Fe^{IV} porphyrin dimers[26,27] and oxo-bridged Fe^{IV} corrole dimers.[28,29] It thus appears that the paramagnetism of the $\{Fe_2(\mu\text{-}O)_2\}$ complexes studied and the maximal spin pairing in high-valent nitrido-bridged heme dimers reflect a difference in the coordination geometry in the two families of dinuclear complexes: an edge-sharing bioctahedral arrangement in the former versus a corner-sharing arrangement in the latter complexes.

Figure 5 presents key optimized geometry parameters for the complexes studied and these are in general in excellent agreement with those found from crystallographic analyses of closely related species. In the optimized structure of $[(bipy)_2Fe(\mu\text{-}O)_2Fe(bipy)_2]^{3+}$, the interatomic distances are Fe–O = 1.825 Å, $Fe–N_{pyridine}$ = 1.990 and 2.074 Å, Fe–Fe = 2.691 Å, and the Fe-O-Fe angle is 95°. These values can be compared with those obtained in a crystallographic analysis of $[Fe_2(\mu\text{-}O)_2(5\text{-}Et_3\text{-}TPA)_2](ClO_4)_3$ (5-Et_3-TPA = tris[(5-ethyl-2-pyridyl)methyl]amine), in which the interatomic distances are Fe–O = 1.827 (average of 1.805(3) and 1.860(3) Å), $Fe–N_{pyridine}$ = 2.003(3) and 2.025(3) Å, Fe–Fe = 2.683(1) Å, and the Fe-O-Fe angle is 94.1°.[11] For $[(bipy)_2Fe(\mu\text{-}O)_2Fe(bipy)_2]^{4+}$, the optimized interatomic distances for the $S=1$ state are Fe–O = 1.794 Å, Fe–N = 1.988 and 2.070 Å, and Fe–Fe = 2.834 Å; for the $S=2$ state Fe–O = 1.826 Å, Fe–N = 1.996 and 2.056 Å, and Fe–Fe = 2.805 Å, which may be compared with Fe K-edge EXAFS best-fit distances for $[Fe^{IV}_2(\mu\text{-}O)_2(bpmcn)_2](OTf)_4$ of 1 O at 1.79 Å, 3 N at 1.99 Å, and 1 Fe at 2.81 Å.[13] Note that while the iron–ligand distances are quite similar for all the $[(bipy)_2Fe(\mu\text{-}O)_2Fe(bipy)_2]^{3+,4+}$ species studied, there are significant variations in the Fe-O-Fe (and O-Fe-O angles). As a result, the Fe–Fe separation in $[(bipy)_2Fe(\mu\text{-}O)_2Fe(bipy)_2]^{4+}$ is slightly longer than that in $[(bipy)_2Fe(\mu\text{-}O)_2Fe(bipy)_2]^{3+}$, in agreement with a similar expansion observed for $[Fe^{IV}_2(\mu\text{-}O)_2(bpmcn)_2](OTf)_4$ compared with $[Fe_2(\mu\text{-}O)_2(5\text{-}Et_3\text{-}TPA)_2](ClO_4)_3$.[11,13] Without elaborating too much, we also note that the optimized geometry parameters for the nitrido-bridged heme dimers studied are also in excellent agreement with relevant crystallographic results. For example, the calculated $Fe–N_{nitrido}$ distances in $[(por)Fe]_2N$ of 1.645 Å and in $[\{(por)Fe\}_2N]^+$ of 1.619 Å agree closely with the corresponding distances of 1.662 and 1.628 Å in the crystal structures of $[(TPP)Fe]_2N$ and $[\{(TTP)Fe\}_2N]^+$ (TTP = *meso*-tetrakis(*p*-tolyl)porphyrin), respectively.[23] The overall excellent agreement between the calculated and observed geometry parameters constitutes powerful evidence that these calculations correctly describe the electronic structures of $\{Fe^{IV}_2(\mu\text{-}O)_2\}$ intermediates and, specifically, that the canonical MOs presented in Figure 1 and Figure 2 provide a correct description (although, of course, not a unique description) of the electron distributions in the relevant experimentally studied species.

Figure 5 also includes key gross atomic-spin populations for the various species studied. As in the case of heme peroxidase compound II models, the unpaired electronic-spin density is entirely concentrated on the Fe and O atoms for all the $\{Fe_2(\mu\text{-}O)_2\}$ model complexes studied, with small minority spin populations on the nitrogen atoms. The Fe/O spin partitioning ratio for $[(bipy)_2Fe(\mu\text{-}O)_2Fe(bipy)_2]^{3+}$ is approximately 3.04 (1.1653/0.3836); for $[(bipy)_2Fe(\mu\text{-}O)_2Fe(bipy)_2]^{4+}$ in the $S=1$ state, 3.29 (0.8122/0.2466) and in the $S=2$ state, 3.68 (1.5978/0.4345). These ratios are considerably higher than the approximately 1:1 ratio calculated for Fe^{IV}-(por)(O)[30,31,32] but similar to a ratio of about 3:1 calculated for $Fe^{IV}(por)(OCH_3)_2$,[33,34] thus indicating that a μ-oxo ligand, like the univalent methoxide ligand, is significantly less able than a terminal oxo ligand to delocalize electronic spin

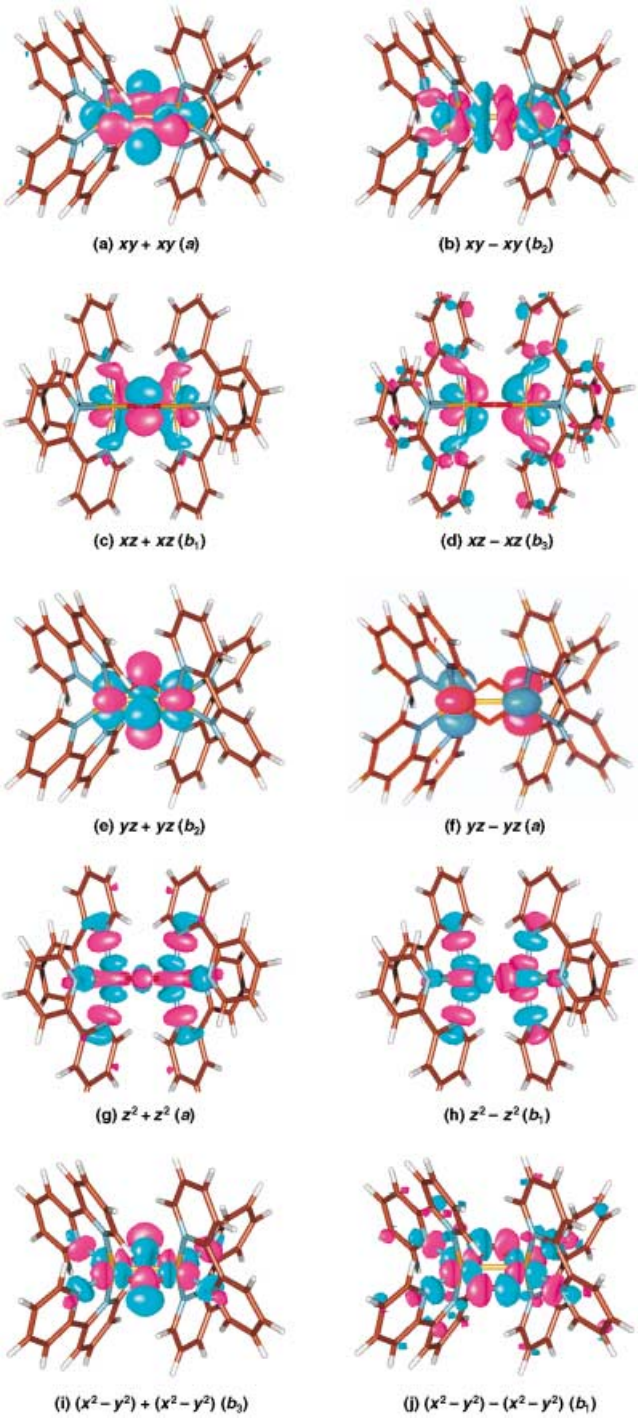

Figure 2. The primarily d-orbital-based α-spin MOs of $[(bipy)_2Fe(\mu\text{-}O)_2Fe(bipy)_2]^{3+}$. The corresponding β-spin MOs exhibit qualitatively similar shapes as the α-spin MOs. The primarily d-orbital-based MOs of the $S=1$ and $S=2$ states of $[(bipy)_2Fe(\mu\text{-}O)_2Fe(bipy)_2]^{4+}$ also exhibit the same qualitative shapes as the MOs depicted here.

density and presumably also positive charge away from high-valent iron centers.

An examination of the Mulliken charges of the three $\{Fe_2(\mu\text{-}O)_2\}$ species studied (Figure 5) provided further insights into this issue. The charges on the Fe, O, N_{axial}, and $N_{equatorial}$ atoms are $+0.890$, -0.632, -0.428 and -0.359 for

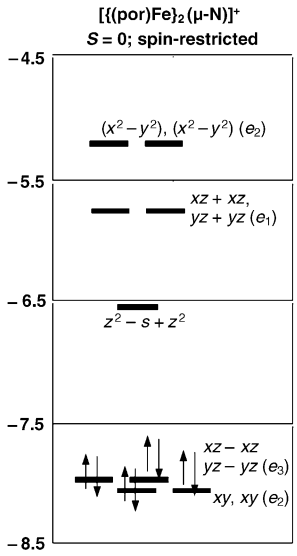

Figure 3. MO energy level diagrams for the nitrido-bridged heme dimers studied. The energy scale is in eV. The numerical values of the orbital energies are listed in the Supporting Information.

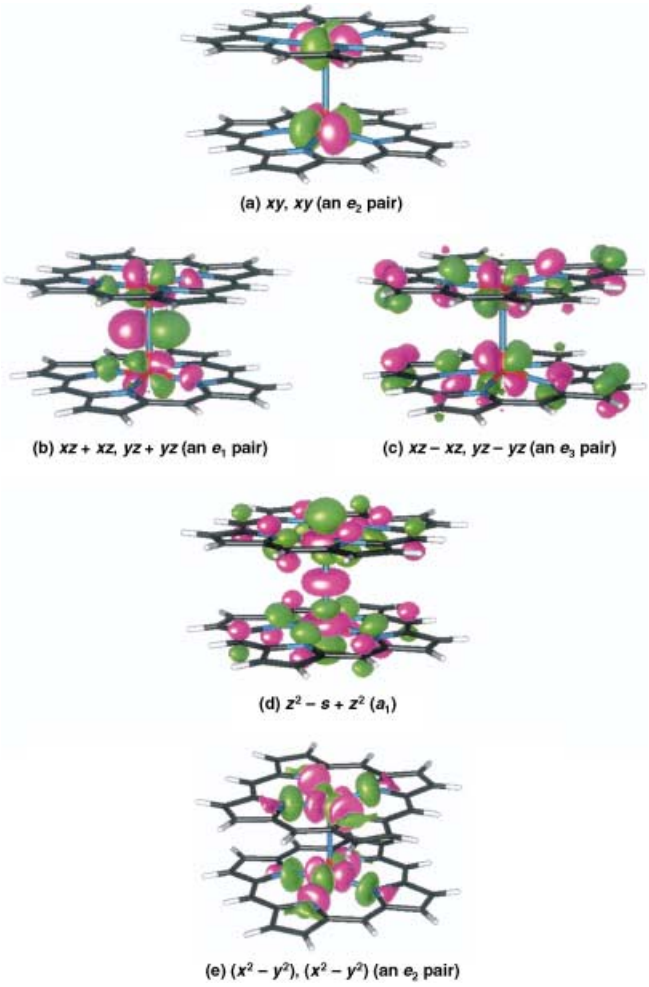

Figure 4. Some primarily d-orbital-based MOs of $[\{(por)Fe\}_2N]^+$ ($S=0$).

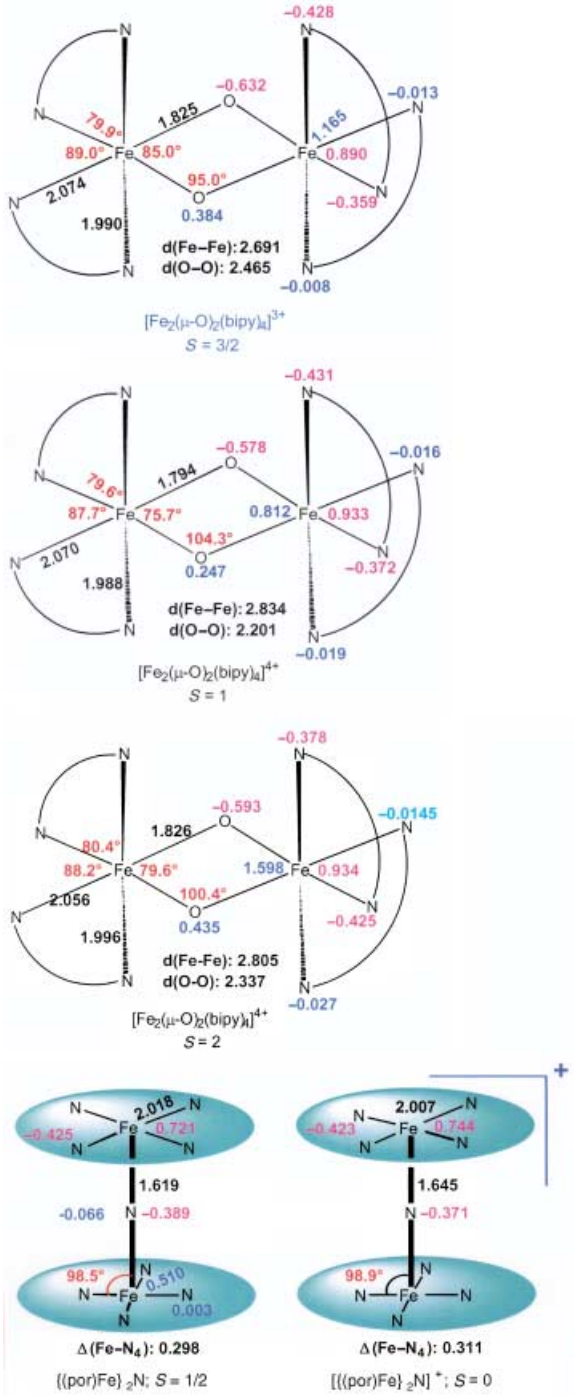

Figure 5. Selected optimized geometry parameters (bond lengths [Å] in black, angles [°] in red), Mulliken charges (magenta), and atomic spin populations (blue) for the molecules studied.

$[(bipy)_2Fe(\mu\text{-}O)_2Fe(bipy)_2]^{3+}$; 0.933, −0.578, −0.431 and −0.372 for the $S=1$ state of $[(bipy)_2Fe(\mu\text{-}O)_2Fe(bipy)_2]^{4+}$; and 0.934, −0.593, −0.425 and −0.378 for the $S=2$ state of $[(bipy)_2Fe(\mu\text{-}O)_2Fe(bipy)_2]^{4+}$, respectively, the equatorial plane being identified with the plane containing the $\{Fe_2(\mu\text{-}O)_2\}$unit. Some noteworthy aspects of these charge distributions are as follows: The equatorial nitrogen atoms carry smaller negative charges than the axial ones, as might be expected from the fact that $Fe{-}N_{equatorial}$ bonds are longer than the $Fe{-}N_{axial}$ bonds. The overall molecular charge density profiles of the +3 and +4 species are not radically different, which is consistent with the electroneutrality principle and reflects the ability of the bipy ligands to delocalize the high positive charges of these ionic species. That said, the total Mulliken electronic charge on the $\{Fe_2(\mu\text{-}O)_2\}$ unit is about 30–40% higher in the $[Fe_2(\mu\text{-}O)_2]^{4+}$ species, relative to the $[Fe_2(\mu\text{-}O)_2]^{3+}$ species, which is a significant difference. Accordingly, the oxygen atoms in the $[Fe_2(\mu\text{-}O)_2]^{4+}$ species may be expected to be much more electrophilic relative to the $[Fe_2(\mu\text{-}O)_2]^{3+}$ species. This has indeed been observed to be the case. Thus, in the context of C–H activation, while $[Fe_2(\mu\text{-}O)_2(tpa)_2]^{3+}$ only reacts with substrates with activated C–H bonds such as ethylbenzene and cumene, $[Fe^{IV}_2(\mu\text{-}O)_2(bpmcn)_2]^{4+}$ was found to react with adamantane at −40 °C under Ar, affording 1-adamantanol and 2-adamantanone in 56% and 20% yield, respectively.[13]

In summary, DFT calculations have provided a framework for understanding the electronic structures of $\{Fe^{IV}_2(\mu\text{-}O)_2\}$ intermediates with locally low-spin metal centers, species that may actually occur in Nature as reactive intermediates of non-heme diiron alkane monooxygenases such as AlkB. The calculations also explain why these intermediates exhibit different ground spin states relative to high-valent μ-nitrido/carbido heme dimers, despite the same formal metal oxidation states. The close agreement between theory and experiment with respect to key geometry parameters provides strong evidence that the calculations presented here faithfully describe the actual electronic structures of the relevant synthetic $\{Fe_2(\mu\text{-}O)_2\}$ intermediates.

Received: April 28, 2003 [Z51768]

Keywords: density functional calculations · iron · O ligands · porphyrinoids

[1] S. J. Lippard, J. M. Breg, *Principles of Bioinorganic Chemistry*, University Science Books, Mill Valley, CA, **1994**.
[2] L. Que, W. B. Tolman, *Angew. Chem.* **2002**, *114*, 1160; *Angew. Chem. Int. Ed.* **2002**, *41*, 1114–1137; Corrigendum: L. Que, W. B. Tolman, *Angew. Chem.* **2002**, *114*, 1900; *Angew. Chem. Int. Ed.* **2002**, *41*, 1821.
[3] V. K. Yachandra, K. Sauer, M. P. Klein, *Chem. Rev.* **1996**, *96*, 2927–2950.
[4] R. L. Lieberman, D. B. Shrestha, P. E. Doan, B. M. Hoffman, T. L. Stemmler, A. C. Rosenzweig, *Proc. Natl. Acad. Sci. USA* **2003**, *100*, 3820–3825, and references therein.
[5] L. Shu, J. C. Nesheim, K. Kauffman, E. Münck, J. D. Lipscomb, L. Que, Jr., *Science* **1997**, *275*, 515–518.
[6] M. Merkx, D. A. Kopp, M. H. Sazinsky, J. L. Blazyk, J. Müller, S. J. Lippard, *Angew. Chem.* **2001**, *113*, 2860–2888; *Angew. Chem. Int. Ed.* **2001**, *40*, 2782–2807.
[7] P. J. Riggs-Gelasco, L. Shu, S. Chen, D. Burdi, B. H. Huynh, L. Que, Jr., J. Stubbe, *J. Am. Chem. Soc.* **1998**, *120*, 849–860.
[8] J. A. Broadwater, J. Y. Ai, T. M. Loehr, J. Sanders-Loehr, B. G. Fox, *Biochemistry* **1998**, *37*, 14664–14671.
[9] R. N. Austin, H. K. Chang, G. J. Zylstra, J. T. Groves, *J. Am. Chem. Soc.* **2000**, *122*, 11747–11748.
[10] Y. Dong, H. Fujii, M. P. Hendrich, R. A. Leising, G. Pan, C. R. Randall, E. C. Wilkinson, Y. Zang, L. Que, Jr., B. G. Fox, K.

Kauffmann, E. Münck, *J. Am. Chem. Soc.* **1997**, *119*, 12683–12684.
[11] H.-F. Hsu, Y. Dong, L. Shu, V. G. Young, Jr., L. Que, Jr., *J. Am. Chem. Soc.* **1999**, *121*, 5230–5237.
[12] A. Ghosh, J. Almlöf, L. Que, Jr., *Angew. Chem.* **1996**, *108*, 770–772; *Angew. Chem. Int. Ed. Engl.* **1996**, *35*, 770; A. J. Skulan, M. A. Hanson, H. -F. Hsu, L. Que, Jr, E. I. Solomon, *J. Am. Chem. Soc.* **2003**, *125*, 7344–7356.
[13] M. Costas, J.-U. Rohde, A. Stubna, R. Y. N. Ho, L. Quaroni, E. Münck, L. Que, Jr., *J. Am. Chem. Soc.* **2001**, *123*, 12931–12932.
[14] S.-K. Lee, B. G. Fox, W. A. Froland, J. D. Lipscomb, E. Münck, *J. Am. Chem. Soc.* **1993**, *115*, 6450–6451.
[15] J. Shanklin, E. B. Cahoon, *Annu. Rev. Plant Physiol. Plant Mol. Biol.* **1998**, *49*, 611–641.
[16] The reaction mechanism and intermediates of sMMO have been extensively studied by DFT. For a recent review, see: V. Guallar, B. F. Gherman, S. J. Lippard, R. A. Friesner, *Curr. Opin. Chem. Biol.* **2002**, *6*, 236–242.
[17] For a review on the mechanism of sMMO, see: D. A. Kopp, S. J. Lippard, *Curr. Opin. Chem. Biol.* **2002**, *6*, 568–576.
[18] For the latest major theoretical paper on the reaction mechanism of sMMO, see: M.-H. Baik, B. F. Gherman, R. A. Friesner, S. J. Lippard, *J. Am. Chem. Soc.* **2002**, *124*, 14608–14615.
[19] For a review of DFT calculations on transition metal-containing enzymes, see: P. E. M. Siegbahn, M. R. A. Blomberg, *Chem. Rev.* **2000**, *100*, 421–438.
[20] For a review of DFT calculations on high-valent transition metal porphyrins and related complexes, see: A. Ghosh, E. Steene, *J. Biol. Inorg. Chem.* **2001**, *6*, 739–752.
[21] For additional technical details, the reader is referred to the ADF program manual, available from: Scientific Computing and Modeling, Department of Theoretical Chemistry, Vrije Universiteit, 1081 HV Amsterdam, The Netherlands.
[22] For the first report of a nitrido-bridged heme dimer, $[(TPP)Fe]_2N$ (TPP = *meso*-tetraphenylporphyrinato), see: D. A. Summerville, I. A. Cohen, *J. Am. Chem. Soc.* **1976**, *98*, 1747–1752.
[23] For a recent study, see: M. Li, M. Shang, N. Ehlinger, C. E. Schulz, W. R. Scheidt, *Inorg. Chem.* **2000**. *39*, 580–583.
[24] A. Ghosh, P. R. Taylor, *Curr. Opin. Chem. Biol.* **2003**, *7*, 113–124.
[25] While an energy difference of 0.85 eV is substantial, we cannot be sure of the exact energy of the $S=0$ state relative to the lower-energy paramagnetic states. The present $S=0$ calculation was carried out in a simple-minded manner by a spin-unrestricted calculation with the assumption that there are no unpaired electrons. A broken-symmetry DFT or an MCSCF (CASSCF) calculation might be considered more meaningful, but as discussed elsewhere [24], even such calculations are unlikely to yield reliable energy differences. More advanced calculations such as CASPT2 or CCSD(T) are currently not feasible for the systems studied. Again, ref [24] provides a critical comparison of all these methods.
[26] D. Mansuy, J.-P. Lecompte, J.-C. Chottard, J.-F. Bartoli, *Inorg. Chem.* **1981**, *20*, 3119–3121.
[27] J. P. Battioni, D. Dupre, D. Mansuy, *J. Organomet. Chem.* **1981**, *214*, 303–309.
[28] E. Vogel, S. Will, A. Schulze Tilling, L. Neumann, J. Lex, E. Bill, A. X. Trautwein, K. Wieghardt, *Angew. Chem.* **1994**, *106*, 771; *Angew. Chem. Int. Ed. Engl.* **1994**, *33*, 731.
[29] E. Steene, T. Wondimagegn, A. Ghosh, *J. Phys. Chem. B* **2001**, *105*, 11406–11413; Erratum: E. Steene, T. Wondimagegn, A. Ghosh, *J. Phys. Chem. B* **2002**, *106*, 5312–5312.
[30] A. Ghosh, J. Almlöf, L. Que, Jr., *J. Phys. Chem.* **1994**, *98*, 5576–5579.
[31] H. Kuramochi, L. Noodleman, D. A. Case, *J. Am. Chem. Soc.* **1997**, *119*, 11442–11451.
[32] A. Dey, A. Ghosh, *J. Am. Chem. Soc.* **2002**, *124*, 3206–3207.
[33] DFT calculations on $Fe^{IV}(por)(OCH_3)_2$: J. Conradie, J. Swarts, A. Ghosh, *J. Phys. Chem. B*, **2004**, *108*, 452–456.
[34] Experimental characterization of $[Fe^{IV}(TMP)(OCH_3)_2]$ (TMP = *meso*-tetramesitylporphyrinato): J. T. Groves, R. Quinn, T. J. McMurry, M. Nakamura, G. Lang, B. Boso, *J. Am. Chem. Soc.* **1985**, *107*, 354–360.

